Article

Not peer-reviewed version

In-Situ Observation on the Grain Growth Behavior and Marten-Sitic Transformation of Supercooled Austenite in NM500 Wear-Resistant Steel at Different Quenching Temperatures

Zhongbo Li , Qing Yuan * , Shaopu Xu , Yang Zhou , Sheng Liu , Guang Xu

Posted Date: 25 April 2023

doi: 10.20944/preprints202304.0909.v1

Keywords: in-situ observation; austenite; martensite; twins; quenching temperature

Article

In-Situ Observation on the Grain Growth Behavior and Martensitic Transformation of Supercooled Austenite in NM500 Wear-Resistant Steel at Different Quenching Temperatures

Zhongbo Li [1,2], Qing Yuan [1,*], Shaopu Xu [2], Yang Zhou [2], Sheng Liu [1] and Guang Xu [1]

[1] State Key Laboratory of Refractories and Metallurgy, Key Laboratory for Ferrous Metallurgy and Resources Utilization of Ministry of Education, Wuhan University of Science and Technology, Wuhan 430081, China; lzb7460377@163.com (Z.L.); liusheng@wust.edu.cn (S.L.); xuguang@wust.edu.cn (G.X.)

[2] Nanyang Hanye Special Steel Co. Ltd, Nanyang 474500, China; lcb-9999@163.com

* Correspondence: yuanqing@wust.edu.cn; Tel.: +86-15994235997

Abstract: In-situ observation on the austenite grain growth and martensite transformation in a developed NM500 wear-resistant steel were conducted on a Confocal Laser Scanning High-temperature Microscope (CSLM). Results indicated that the martensite nucleation did not synchronously proceed during quenching process. The selective prenucleation dominated in martensite nucleation, which dividing untransformed austenite into several regions, and resulting in the larger size of fresh martensite. Martensite can not only nucleate at parent austenite grain boundaries, but also nucleate in the preformed martensite laths and twins. Smaller constraint in the martensite growth was achieved in a larger parent austenite grain size, leading to the longer fresh martensite and secondary martensite. Besides, the transformation kinetics of martensite was accelerated in a higher quenching temperature. Moreover, the martensitic laths presented in parallel laths (0~2°) based on the pre-formed lath or distributed in triangle, parallelogram or hexagon with an angle of 60° or 120°. Interestingly, martensitic lath also traversed the unstable new parent austenitic grain boundaries. In addition, the size of austenite grains increased with the quenching temperature, and austenite grains coarsened in a short time at a higher quenching temperature of 1160 ℃. Furthermore, a large amount fine dispersed particles redissolved and ripped at 1160 ℃, resulting in the many large and visible carbonitrides.

Keywords: In-situ observation; austenite; martensite; twins; quenching temperature

1. Introduction

Wear, fracture and corrosion are usually the main failure modes in the service of metal materials. However, compared with fracture and corrosion, wear will not directly cause the failure of metal parts. However, equipment parts are difficult to repair due to wear, and frequent replacement significantly reduces the working efficiency and service life of equipment, thus leading to a large amount of material and energy loss [1–4]. At present, among the metal wear-resistant materials, austenitic high manganese (Mn) steel, high chromium (Cr) cast iron and low alloy wear-resistant steel are the most widely used. Among them, austenitic high-manganese steel has the surface austenitic structure which can induce phase transition (TRIP effect) under the strong extrusion or impact, and quickly produce work hardening. Whereas the core of austenitic high-manganese steel still retains the good toughness and plasticity because of the austenitic structure [5–7]. However, austenitic high-manganese steel just shows excellent wear performance under high stress and large impact wear conditions, while its wear resistance is relatively weak under low or medium stress conditions, which severely limits the application scope of austenitic high-manganese steel in the wear-resistant materials field [8]. As the second-generation wear-resistant material, high chromium cast iron is currently recognized as the best wear-resistant material, showing excellent wear-resistant properties under abrasive wear conditions [9–11]. The feature of high chromium cast iron is many non-network carbide M7C3 with hardness of 1600HV is precipitated in the material matrix. The strength and

hardness are enhanced by the second phase particles, and the toughness and plasticity of high chromium cast iron is better than that of white cast iron [12]. Therefore, high chromium cast iron has good wear resistance under various working conditions, and its mechanical equipment can also meet the needs of long-term wear in complex environments. However, due to the large number of valuable elements such as Cr and nickel (Ni), the production process of high chromium cast iron is complex, which promotes the production cost of this wear-resistant material and then limits its wide application in industrial production [13]. In view of many problems about service and production of austenitic high manganese steel and high chromium cast iron, common alloy wear-resistant steel has gradually become the research topic of the new generation of wear-resistant metal materials, especially the low-alloy wear-resistant steel [14–18].

At present, various brands of wear-resistant steel products prevailed in Chinese iron and steel manufacturers, among which the production technology of the products below NM400 was relatively mature. The tempered martensite was obtained by off-line re-austenitizing after rolling to improve the strength hardness, and then the toughness was improved by subsequent tempering. Martensite has ultra-high strength and hardness among the different microstructures in steel, and it is usually selected as an important microstructure in the production of high strength steel and ultra-high strength steel. Therefore, in all kinds of low-alloy wear-resistant steel products, martensitic wear-resistant steel is promising. Martensitic wear-resistant steel had been able to replace high-manganese austenitic wear-resistant steel under medium and low stress. Martensite provided the main wear resistance relied on its high hardness, but the wear resistance under high impact was erratic due to its poor toughness. Therefore, many studies on martensitic wear-resistant steel focused on improving the toughness and plasticity of martensitic laths [19–21].

There has been much research on the toughness and plasticity control unit of martensitic. By analyzing the relationships between austenitic grain size, martensitic lath, block, packet, and strength-toughness of martensitic steel, it revealed that martensitic lath and block were the organizational unit affecting the strength and hardness, while the martensitic packet yielded the plasticity and toughness [22,23]. By observing the crack propagation in martensitic steel, Liang et al. found that the crack propagation could be effectively inhibited by the smaller size and angle of the martensitic packet [24]. The main structure control unit affecting fracture, the size of martensitic block, was identified by Inoue et al. through the study on the cleavage fracture of tempered martensitic steel [25]. Although there were many investigations on the toughness and plasticity of martensitic, the relevant conclusions were all accidental, and the exact mechanism on the toughness and plasticity control unit of martensitic steel was not clearly revealed. In addition, some scholars improved the fracture toughness and elongation of martensitic steel by optimizing the composition and heat treatment process, so that about 30% residual austenite were obtained at room temperature. The residual austenite distributed among martensitic lath in a thin film, which improved the fracture toughness and elongation of martensitic steel [26].

In addition, the wear resistance of martensitic steel had been studied extensively. Liang et al. reported that low-alloy martensitic wear-resistant steel exhibited better wear resistance than austenitic high-manganese steel under the condition of moderate impact wear, and its comprehensive mechanical property was more than twice that of austenitic high-manganese steel [27]. Furthermore, they declared that the relative wear resistance of martensitic wear-resistant steel with the same carbon content could be effectively improved by increasing the volume fraction of martensitic lath. Cao et al. prepared Ti-Cr-B microalloyed high-strength wear-resisting steel with tempered martensite. In which, the high dislocation density and tempered carbide precipitations hardened the matrix [28]. In the work of Ma et al., they studied the composition, properties, microstructure and wear resistance of the subsurface of martensitic wear-resistant steel after abrasive wear, and found that the solid solution carbon content in martensitic structure was a direct factor affecting the wear resistance and subsurface hardness [29].

Research on the high grade low-alloy wear-resistant steel are insufficient. A high grade NM500 wear-resistant steel was presented in the present study. It has been verified that the heat treatment process has a great influence on the microstructure and properties of low-alloy wear-resistant steel.

Preprints (www.preprints.org) | NOT PEER-REVIEWED | Posted: 25 April 2023 doi:10.20944/preprints202304.0909.v1

Martensitic transformation was the main means to strengthening steel during heat treatment. The theory of martensitic transformation was closely related to its heat treatment. The determination of quenching temperature and subsequent cooling in quenching process played a decisive role in the microstructure and properties of steel. However, the dynamic investigation on austenite grain growth and martensite transformation in NM500 wear-resistant steel was missing. Therefore, the phase transformation behavior of NM500 wear-resistant steel in continuous cooling process was analyzed by Confocal Laser Scanning High-temperature Microscope (CSLM). Results in present study will provide more lifesome austenite grain growth and martensite transformation with different quenching temperatures.

2. Experimental Procedures

Figure 1 shows the VL2000DX-SVF17SP confocal laser scanning high-temperature microscope and the corresponding quenching process. This CSLM equipment generally consisted of flow control device, console, display and high temperature microscope, etc., which can observe and capture all kinds of physical and metallurgical phenomena in real time. It guaranteed the dynamic process and high resolution without loss of real time through high-speed laser scanning imaging. A higher automation degree was achieved through digital image information storage and processing technology. The light source of CSLM was He-Ne laser, whose wavelength and resolution were about 632.8 nm and 0.25μm, respectively. Various phases emerged under the effect of thermal etching, rather than chemical corrosion.

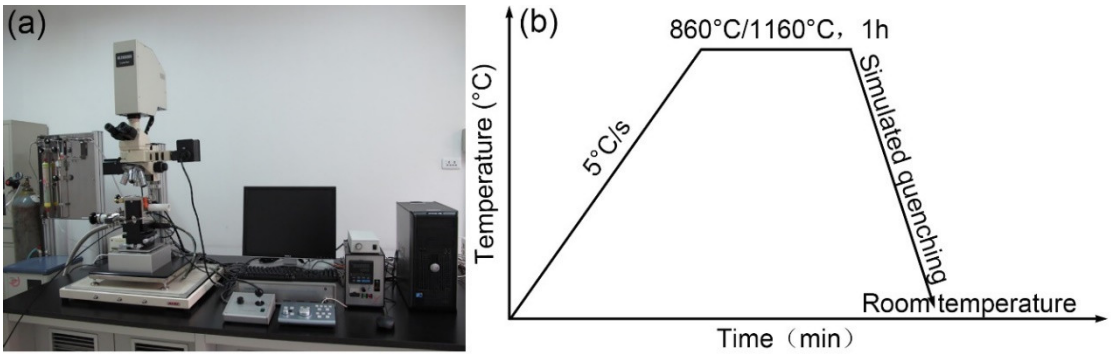

Figure 1. (**a**) The confocal laser scanning high-temperature microscope and (**b**) in-situ observation process.

The experimental steel was a developed high-grade NM500 steel with a chemical composition of Fe-0.23C-0.20Si-1.49Mn-1.15Cr-0.25Ni-0.37(Nb+V+Ti+Mo)-0.022Cu-0.00174B-0.01P-0.002S. Small cylindrical sample with a dimension of Φ6mm×5mm was finish machined, and the two faces of the sample were polished until the mirror surface. Subsequently, the sample was putted into the Al2O3 crucible for in-situ observation. In situ observation experiments with two different quenching temperatures of 860 ℃ and 1160 ℃ were designed according to the tempering process in industrial production. Before the experiment, the sample chamber was vacuumed to 6×10-3 Pa, and then argon gas was introduced to prevent the sample oxidation. The system can automatically shoot high-definition pictures and generate video files of microstructure evolution to record the dynamical process of microstructure evolution in real time during the experiment. In addition, to facilitate the analysis of grain size evolution, the eyepiece will be manually changed during the in-situ observation experiment and the appropriate magnification will be selected due to the different grain size of PAGs caused by the quenching temperature of 860 ℃ and 1160 ℃. Figure 1b demonstrates the heating process with two different quenching temperatures. Firstly, the samples were reheated to 860 ℃ and 1160 ℃ respectively with a rate of 5 ℃/s and then held for 1 h. Subsequently, the maximum cooling rate was applied to cool the specimens to the room temperature after thermal holding to simulate the quenching process. Microstructure evolution was recorded throughout the whole process with a recording frequency of 5 photos/s.

 doi:10.20944/preprints202304.0909.v1

3. Results and Discussion

3.1. Austenite Nucleation

Figure 2 manifests the morphologic changes of the sample from room temperature to preset temperature of 860 °C. Some dark particles existed on the surface of the sample, and these dark particles were likely to be the second phase precipitates with a larger size (Figure 2a). When the temperature increased to 548.7 °C, some corrugated folds began to appear on the surface of the bright sample. These folds were the grain boundaries of the initial ferrite (pearlite) of the sample, which gradually emerged under the condition of thermal etching (Figure 2b). As the temperature increased to 701.6 °C, another corrugated fold gradually covered the grain boundaries of the existing ferrite (Figure 2c). And this corrugated fold became more and more clear and gradually formed the grain boundaries of polygonal grains as the temperature continued to rise to 827.7 °C (Figure 2d) and 862.9 °C (Figure 2e). It was inferred that the corrugated fold at 701.6 °C was austenitic grain boundary, that is, the Ac1 temperature (the beginning temperature at which the pearlite transforms to austenite during heating process) was about 701.6 °C when the steel was reheated at 5 °C/s. The measured Ac1 temperature of this experimental steel was about 658 °C using thermal simulated test, but the Ac1 temperature obtained via in-situ observation was apparently higher. This was because the measured Ac1 temperature was obtained with a very slow heating rate (about 0.1 °C/s), and the measured Ac1 temperature increased with the increase of the heating rate (5 °C/s). Moreover, sample fleetly finished the austenization process with a faster heating rate. When the temperature was 862.9 °C (Figure 2e), the austenization process completed, but the grain boundary morphology of the initial microstructure remained. At this time, the visible black precipitates became clearer and their size increased.

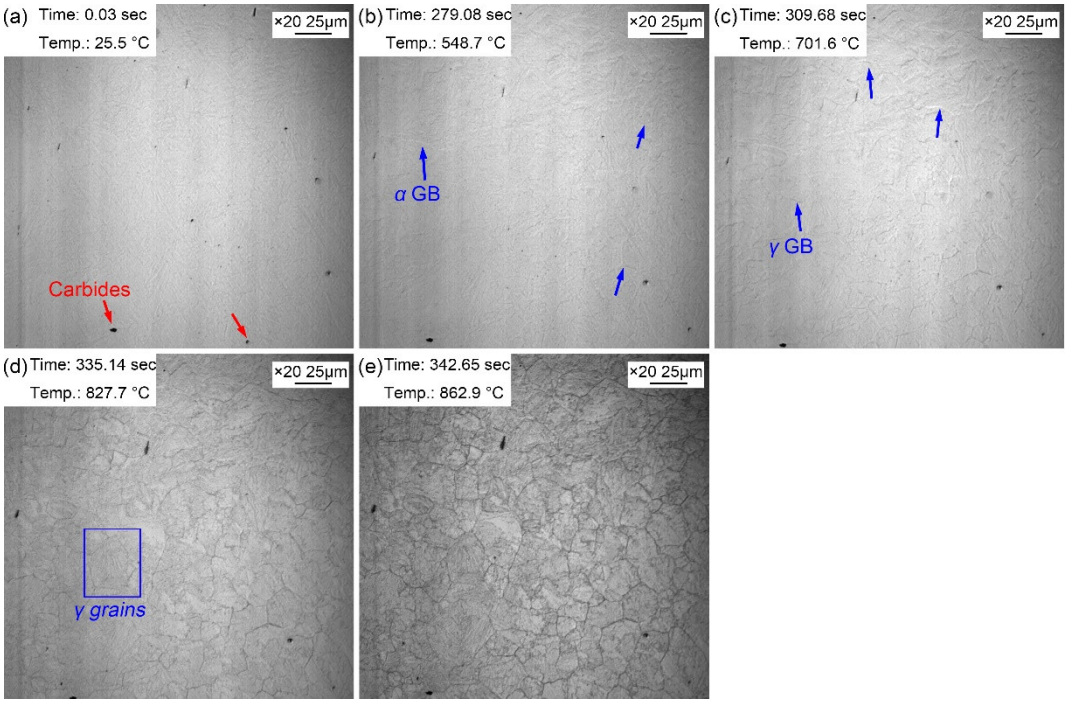

Figure 2. Morphology variations from room temperature to 860 °C. (**a**) 25.5 °C, before heating; (**b**) 548.7 °C, initial grain boundaries appeared; (**c**) 701.6 °C, austenization began; (**d**) 827.7 °C, obvious austenite grains; (**e**) 862.9 °C, the preset quenching temperature.

Austenite transformation is related to nucleation rate and growth rate, which can be expressed as Equations (1) and (2) [30,31]:

$$N = f_N \exp\left(-Q_N / K\Delta T\right) \quad (1)$$

$$G = f_G \exp\left(-Q_G / K\Delta T\right) \quad (2)$$

Preprints (www.preprints.org) | NOT PEER-REVIEWED | Posted: 25 April 2023 doi:10.20944/preprints202304.0909.v1

Where, N is the nucleation rate, G is the growth rate, Q_N and Q_G are the nucleation and growth activation energies, f_N and f_G are the impact factors between structure and nucleation with growth, and ΔT is the superheat. It reveals that the superheat increased with the increase of the heating rate, which increased the nucleation rate and growth rate of austenitic transformation. Therefore, the rate of austenitic transformation increased significantly, and the time required from the initial to complete austenitizing was greatly reduced, and then the required phase transition interval was correspondingly reduced. In addition, the transformation of steel during continuous heating can be equivalent to the accumulation of countless isothermal transformations. The relationship between isothermal incubation period and transition temperature can be established using Scheil superposition principle [32].

$$\sum_{i=1}^{i=n} \frac{\Delta t}{A_i} = 1 \tag{3}$$

Differential Equation (4) was obtained when Δt was small enough.

$$\int_{t=0}^{t=t_n} \frac{dt}{A(T)} = 1 \tag{4}$$

Where, Δt and dt are the transformation time at temperature T, A_i and $A(T)$ are the corresponding incubation period. The relationship between incubation period and transition temperature in the inverse eutectic transition is shown in Equation (5):

$$\int_{T_1}^{T_s} \frac{dt}{A(T)} = \int_{T_1}^{T_s} \frac{1}{A(T)} \cdot \frac{1}{\frac{dT}{dt}} \cdot dT = \int_{T_1}^{T_s} \frac{1}{A(T)} \cdot \frac{1}{v} \cdot dT = 1 \tag{5}$$

Relationships between transformation rate C, transformation beginning and ending temperatures T_s and T_f, and heating rate v are interpreted by Equations (6) and (7) when transformation volume is f.

$$c = \frac{df}{dt}, v = \frac{dT}{dt} \tag{6}$$

$$\int_{t=0}^{t=t_n} \frac{df}{dt} dt = \int_{T_s}^{T_f} \frac{df}{dt} \cdot \frac{dT}{v} = \int_{T_s}^{T_f} \frac{C}{v} \cdot dT = 1 \tag{7}$$

Where, T_1 is equilibrium temperature, t_n is the time to the transformation ending temperatures T_f. It proves that with the increase of the heating rate, both the initial temperature and the end temperature of the phase transition increased. In addition, the dissolution and diffusion of carbonitrides was inevitable during the austenitizing process of experimental steel, and atoms migrated between phases through the diffusion mechanism. With the increase of heating rate, the diffusion of carbon and alloying elements at equilibrium temperature decreased, thus increasing the austenitic transition temperature. In the process of continuous heating, with the increase of temperature, the diffusion coefficient of atoms increased greatly, and the diffusion rate of atoms accelerated significantly, so that the driving force of austenite phase transformation was obviously enhanced.

The morphologic variation of the sample from room temperature to preset temperature of 1160 °C is displayed in Figure 3. Some dark particles basically determined to be the second phase precipitates appeared on the surface of the sample (Figure 3a). Some corrugated folds began to appear on the surface of the bright sample when the temperature increased to 550.4 °C (Figure 3b). As the temperature increased to 704.7 °C (Figure 3c), another corrugated fold gradually covered the grain boundaries of the existing ferrite structure. The corrugated fold became more and more clear and gradually formed the grain boundaries of polygonal grains when the temperature was 828.4°C (Figure 3d). It was inferred that the corrugated fold at 704.7 °C was austenitic grain boundaries as well. The temperature for the grain boundary appeared was basically the same as that in specimen

Preprints (www.preprints.org) | NOT PEER-REVIEWED | Posted: 25 April 2023 doi:10.20944/preprints202304.0909.v1

reheated to 860 °C. This was because the heating process of the two samples were the same before heating to 860 °C. However, when the sample was reheated to 1160 °C (Figure 3e), more large size grains appeared accompanied with the disappeared small size grains and the grain boundaries became sharper and clearer. In addition, clearly visible second phase precipitated particles increased significantly, and its size has gradually coarsened. It can be explained by the gradual dissolution of some invisible fine dispersed second phase particles when heating from 828.4 °C to 1160 °C, which increasing of austenite grain boundary mobility and then resulting in the partitioning of small grains and the coarsening of austenite grains quickly. It is clear that the increase amount of the second phase precipitated particles was attributed to the insufficient thermal stability in some second phase precipitated particles at high temperature. Compared with the sample quenched at 860 °C, the austenite grains of the sample quenched at 1160 °C coarsened obviously.

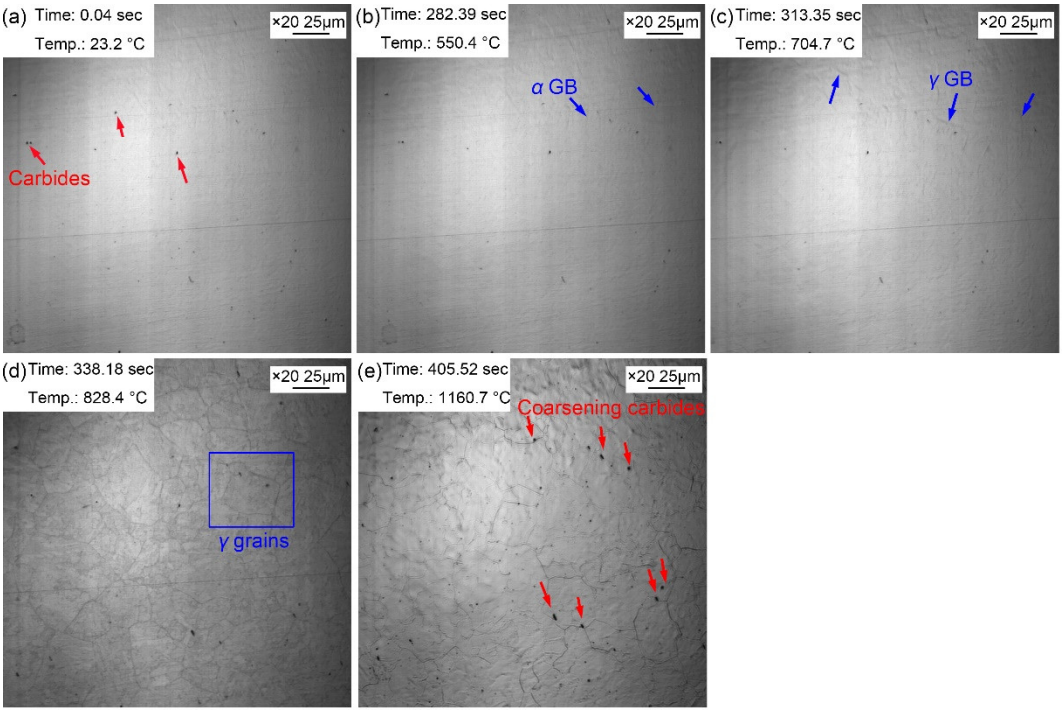

Figure 3. Morphology variations from room temperature to 1160 °C. (**a**) 23.2 °C, before heating; (**b**) 550.4 °C, initial grain boundaries appeared; (**c**) 704.7 °C, austenization began; (**d**) 828.4 °C, obvious austenite grains; (**e**) 1160.7 °C, reached the preset quenching temperature.

3.2. Austenite Growing

Figure 4 shows the morphologic changes of the sample from 1~10 minutes with a time interval of 1 min when the quenching temperature was 860 °C. Compared with the morphology just reheated to the preset temperature, the grain boundaries of austenite grains were clearer after being held at 860 °C for 1 min (Figure 4a). This is because grain boundary grooves would be more easily exposed under the condition of longer thermal etching. In addition, the austenite grain boundaries were narrow and straight with a grain boundaries angle of 120°. Some local small grains gradually merged into large ones during the holding, as shown in the rectangular (Figure 4f,j). In addition, austenite grain boundaries also expanded and migrated to form large grains during the holding, as shown by pink arrows (Figure 4d,j). The gradual merging of small grains and migration of some grain boundaries indicated that grain growth occurred gradually during the process of thermal holding, but the growth process and trend were not obvious.

Preprints (www.preprints.org) | NOT PEER-REVIEWED | Posted: 25 April 2023 doi:10.20944/preprints202304.0909.v1

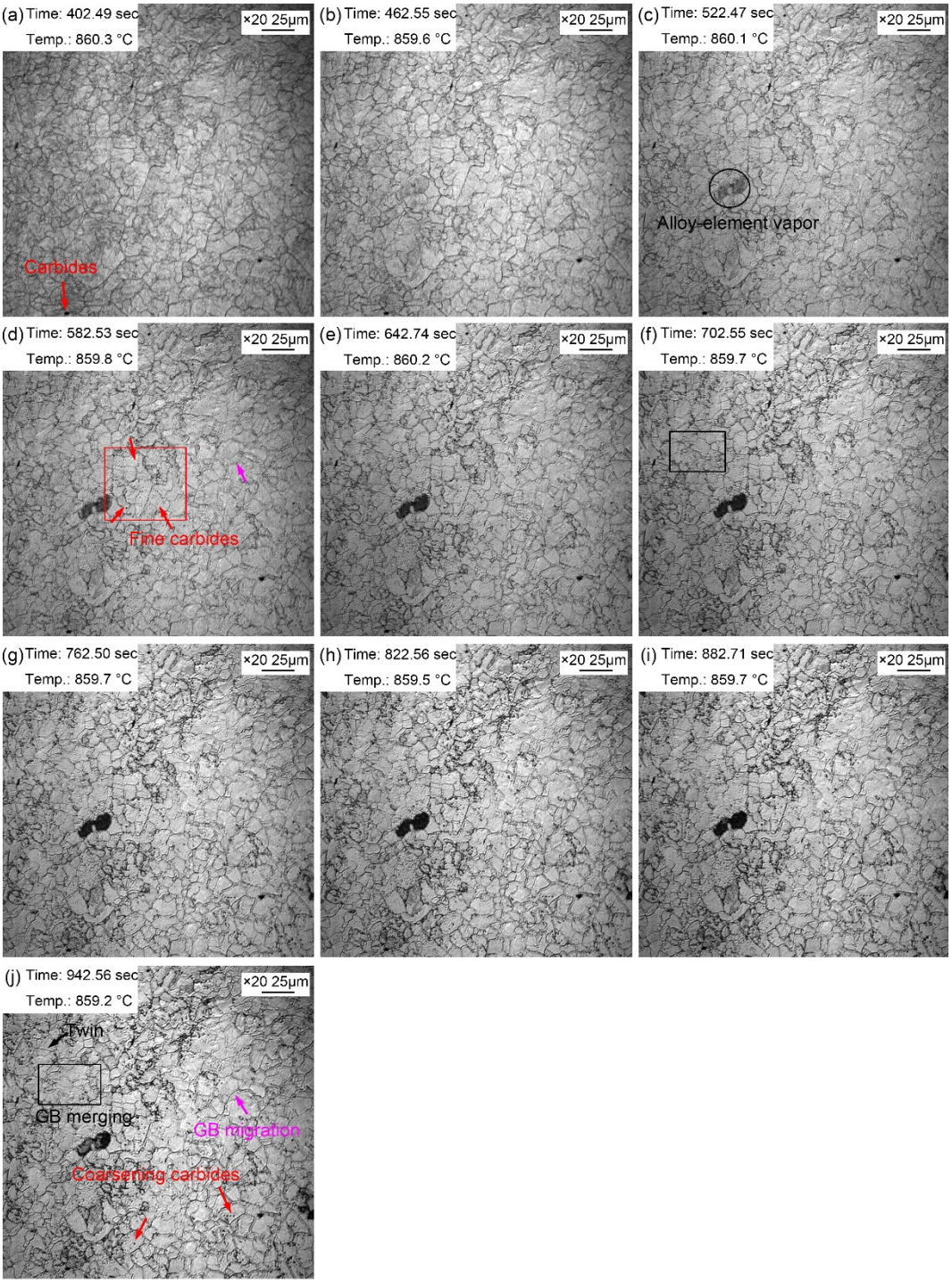

Figure 4. Morphologies during thermal holding at 860 ℃ from 1~10 minutes. (**a**) 1 min; (**b**) 2 min; (**c**) 3 min; (**d**) 4 min; (**e**) 5 min; (**f**) 6 min; (**g**) 7 min; (**h**) 8 min; (**i**) 9 min; (**j**) 10 min.

During the thermal holding process, the dark fog-like substance shown by the oval in Figure 4c appeared. The dark fog-like substance gradually turned black, and then disappeared in the subsequent holding process. This dark mist was the vapor of alloying elements, and some of which tend to steam outward from the steel matrix when reheated. In addition to the clearly visible precipitates at the reheating beginning, many fine dispersed particles also appeared in the austenite grains during the thermal holding, as shown in Figure 4d. These fine second phase particles gradually appeared because part of the nano-second phase particles matured and gradually emerged, and some of the unprecipitated second phase particles gradually precipitated from the matrix. The second phase particles matured during the thermal holding, as shown in Figure 4j.

Preprints (www.preprints.org) | NOT PEER-REVIEWED | Posted: 25 April 2023 doi:10.20944/preprints202304.0909.v1

The morphologic variation with a time interval of 10 min from 20~60 minutes at the quenching temperature of 860 °C is exhibited in Figure 5. Compared with morphology in the holding time of 10 min, the coarsening of the second phase particles was more obvious, and there were more areas where small grains merged into large grains. In addition, twin crystals could be observed in austenite grains (Figure 5a). The existing dark fog-like steam gradually volatilized and disappeared during the thermal holding, while at the same time, the dark fog-like steam appeared in other areas. It may be explained by the uneven distribution of some alloying elements. Besides, the austenite grain coarsening was obvious during the thermal holding, in which the proportion of small grains decreased gradually, and the volume fraction of large grains increased significantly. Moreover, and the intramural twins were more clearly visible (Figure 5e). The intracrystalline twins in this sample can be considered as annealing twins. There were more alloying elements in the steel, which significantly reduced the stacking fault energy. Compared with ordinary carbon steel, intracrystalline twins were more likely to occur in alloyed steels. The appearance of twins segregated and refined the grains, thus increasing the resistance of dislocation movement, and then strengthening the steel.

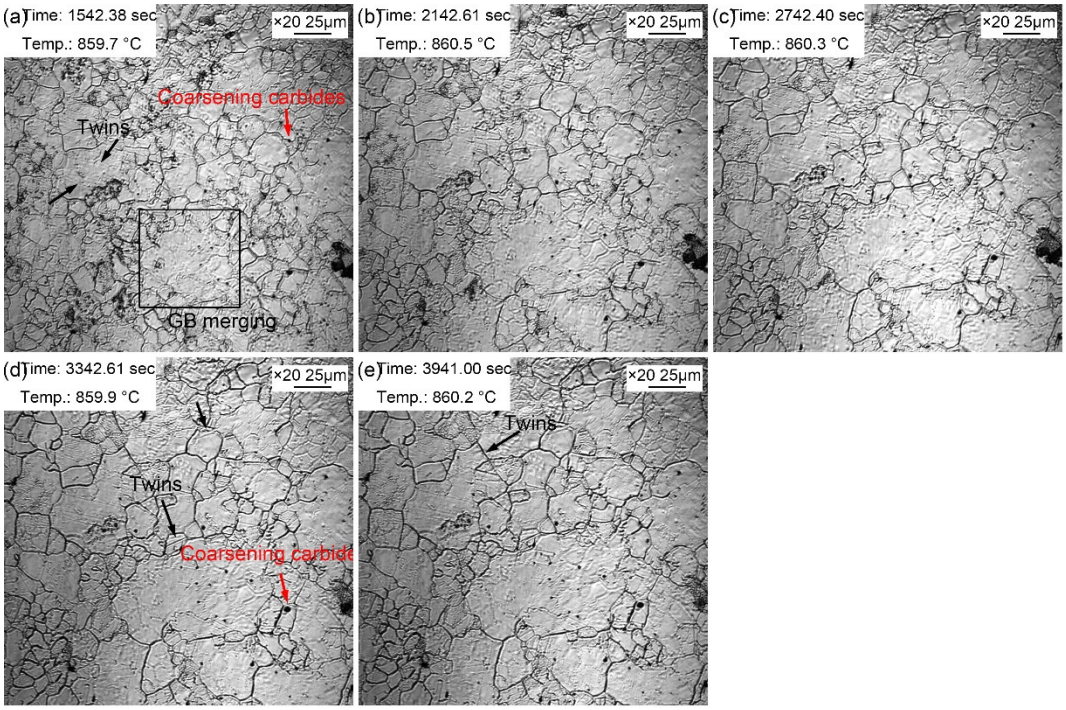

Figure 5. Morphologies during thermal holding at 860 °C from 20~60 minutes. (**a**) 20 min; (**b**) 30 min; (**c**) 40 min; (**d**) 50 min; (**e**) 60 min.

Figure 6 presents the morphologic evolution of the sample from 1~10 minutes at the quenching temperature of 1160 °C with a time interval of 1 minute. Compared with the sample just reheated to the preset temperature, the grain boundaries of austenite grains were much clearer after holding at 1160 °C for 1 min (Figure 6a) by the continuous thermal etching. The migration of grain boundaries was obvious with the extension of holding time, as shown in Figure 6a→6b (blue arrow 1) and 8b→8c (blue arrow 2). Part of the original grain boundaries gradually faded away during the process of grain boundary migration, and the old ones were gradually filled in, leaving only a few traces. In addition, except the outward expansion of grain boundaries, there was an obvious phenomenon that small grains were partitioned by surrounding large grains, as shown in the oval in Figure 6d. The alloy element steam as shown in Figure 5c also appeared during the thermal holding process in specimen reheated to 1160 °C. The alloy element steam gradually turned black, and then disappeared in the subsequent holding process. Besides, many annealing twins traversing the whole grain or occupying the whole grains were captured in the austenite grains. The second phase particles ripened during the holding process, as shown in Figure 6j. The gradual appearance of fine second phase particles during the thermal holding was attributed to the ripening of nanoparticles at 1160 °C, which was

 doi:10.20944/preprints202304.0909.v1

captured by limited magnification. Comparing with the grain morphology at 860 ℃ for 20~60 minutes, the grain size was obviously coarsened when the quenching temperature was 1160 ℃, and the number of small grains was very small. The coarsen second phase particles increased obviously at 1160 ℃, and there were many dense fine second phase particles inside the grain. The microalloying elements in steel were mainly Ti and V. Some small particles precipitated and gradually dissolved into the matrix at 1160 ℃, while some dispersion particles with excellent thermal stability ripened and exposed by thermal etching. Firstly, according to the formula of solid solubility product, some carbonitride particles redissolved in the matrix due to the increase in temperature. In addition, since the solute concentration around small particles was greater than that around large particles, the solute atoms spread from small particles to large particles, resulting in the redissolution of small particles and growing in larger particles. Therefore, the fine precipitates gradually redissolved, and continuously formed large size carbonitride particles when the holding time was long enough at 1160 ℃.

The coarsening of austenite grains at 1160 ℃ was related to the redissolution of the second phase particles. Firstly, the atomic size of V/Ti was very different with Fe, which has a certain solute atomic dragging effect. Reconcentration of a large number of solute atoms such as vanadium (V) and titanium (Ti) at grain boundaries or subgrain boundaries could prevented the migration of grain boundaries and thus inhibited recrystallization. In addition, the second phase particles preferentially precipitated at grain boundaries and dislocation lines, pinning the austenite grain boundaries and hindering the growth of austenite grains. The grain boundary migration was the essence of austenite grain growth. The surface energy increased when grain boundaries contacted with the second phase precipitated particle. Only when the thermal activation energy was greater than the increment of surface energy, the second phase particles will be cut or bypassed by the grain boundary. Therefore, the second phase particles significantly slowed down the formation rate of austenite and prevented the growth of grains.

Preprints (www.preprints.org) | NOT PEER-REVIEWED | Posted: 25 April 2023 doi:10.20944/preprints202304.0909.v1

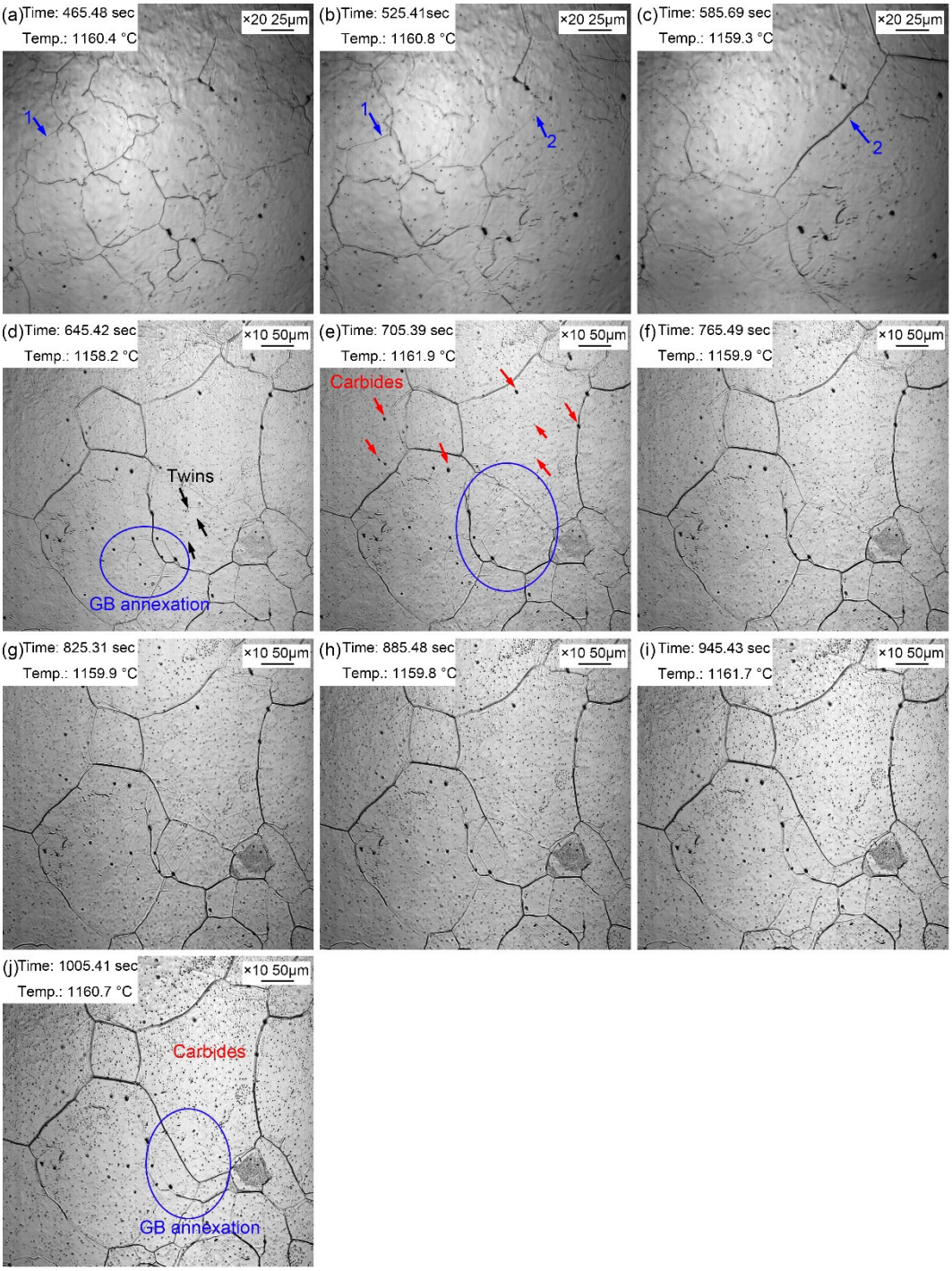

Figure 6. Morphologies during thermal holding at 1160 °C from 1~10 minutes. (**a**) 1 min; (**b**) 2 min; (**c**) 3 min; (**d**) 4 min; (**e**) 5 min; (**f**) 6 min; (**g**) 7 min; (**h**) 8 min; (**i**) 9 min; (**j**) 10 min.

Figure 7 displays the morphologic changes with a time interval of 10 min from 20 to 60 minutes at the quenching temperature of 1160 °C. Dense small black particles formed in the austenite grains. It signified that the coarsening of the second phase particles was more obvious compared with those during the holding time of 10 minutes. In addition, the grain boundaries of small-size austenite were gradually absorbed by the surrounding large-size austenite. Besides, apparent twins were observed in austenite grains (Figure 7a). The dark fog-like steam gradually volatilized and disappeared with the extension of holding time. Furthermore, austenite grain coarsening still occurred during the holding at 20~60 min, in which the proportion of small grains furtherly decreased, and the volume

Preprints (www.preprints.org) | NOT PEER-REVIEWED | Posted: 25 April 2023 doi:10.20944/preprints202304.0909.v1

fraction of large grains significantly increased. The intra twins were more clearly visible (Figure 7e) because of the larger austenite grains.

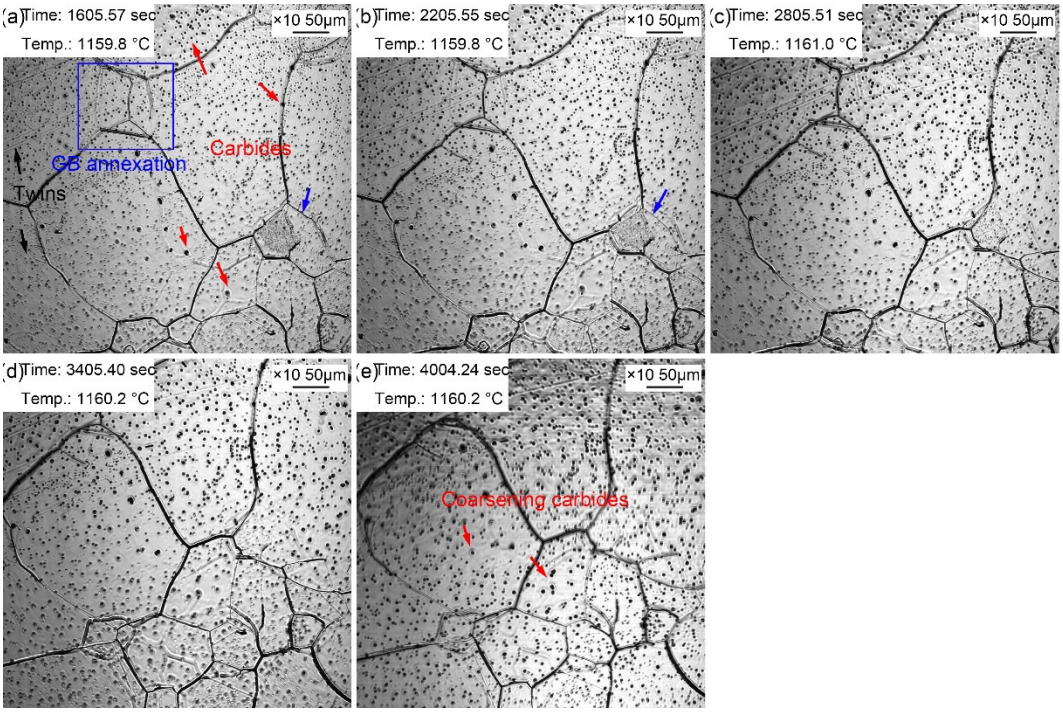

Figure 7. Morphologies during thermal holding at 1160 °C from 20~60 minutes. (**a**) 20 min; (**b**) 30 min; (**c**) 40 min; (**d**) 50 min; (**e**) 60 min.

3.3. Grain Size

Figure 8 summaries the grain size and growth rate of austenite from the formation of austenite to the thermal holding under different quenching temperatures. Enough grains should be ensured to improve the statistical accuracy in the statistical process. Grains less than half a grain were not counted, and grains larger than half were considered as a grain. There was little difference in austenite grain size under two different quenching temperatures during the reheating stage before preset quenching temperatures. However, the austenite grain size in specimen reheated to 860 °C was always smaller than those in the sample with a quenching temperature of 1160 °C. Figure 8b shows the growth law of austenite grains with time when the quenching temperature was 860 °C. The growth process was relatively slow, and the obvious coarsening of austenite grains was completed after holding for about 30 min. The growth process of austenite grains was very rapid and intense, and the coarsening of austenite grains has been completed within 10 minutes at the quenching temperature of 1160 °C. Austenite grain growth rate curves at different quenching temperatures were obtained through the first derivative of austenite grain size and holding time (Figure 8b,d). The austenite grain growth rate was significantly faster when the quenching temperature was 1160 °C than that at 860 °C. In addition, when the quenching temperature was 1160 °C, the maximum austenitic growth rate appeared at the holding time of ~3 min, whereas the maximum austenitic growth rate occurred at ~30 min when the quenching temperature was 860 °C.

Preprints (www.preprints.org) | NOT PEER-REVIEWED | Posted: 25 April 2023 doi:10.20944/preprints202304.0909.v1

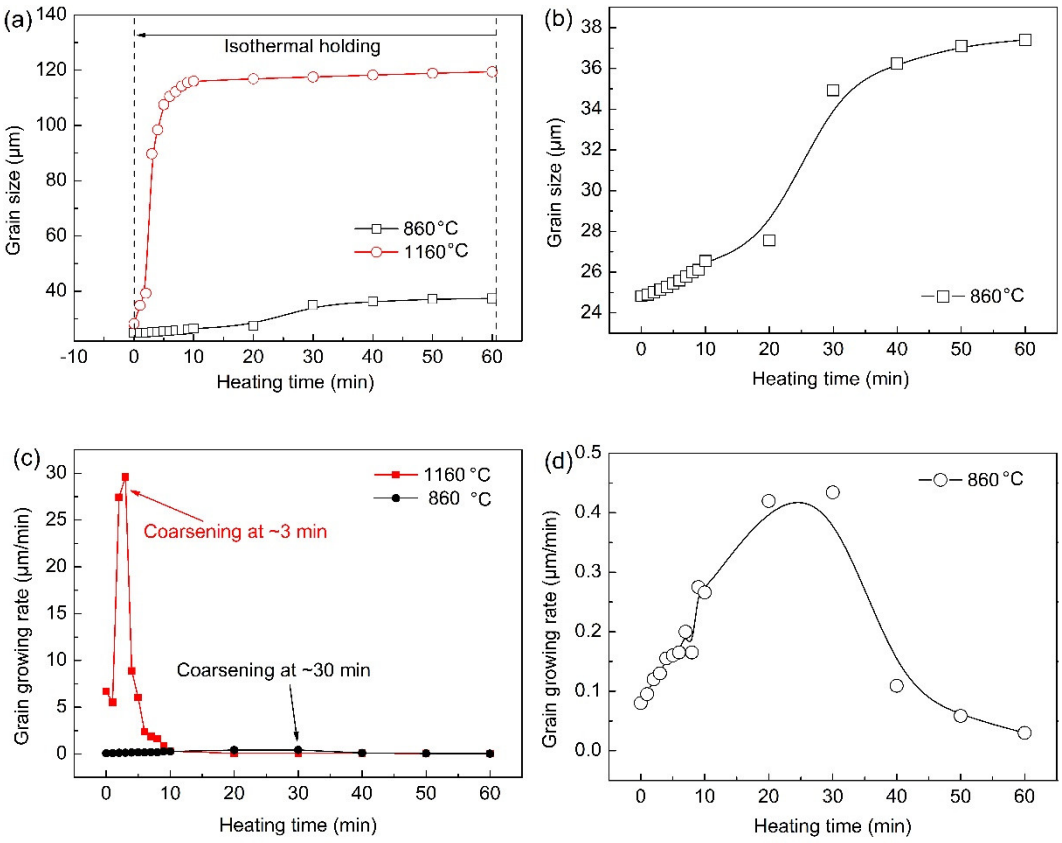

Figure 8. (**a**,**b**) Grain size and (**c**,**d**) growth rate of austenite from the formation to the thermal holding under different quenching temperatures.

According to the growth rules of austenite grains at different quenching temperatures, it can be concluded that the austenite grains coarsened in a short time and the coarsening rate was larger at a higher quenching temperature. This is because the austenite grain boundary migration ability was stronger at a higher temperature. The atomic diffusion process was more rapid, and part of the grain boundary was more easy to fade and disappear. In addition, many small dispersed second phase particles redissolved and ripped, which leaded to a significant decrease in the migration ability of austenite grain boundaries, so that austenite grain boundaries freely expanded. Furthermore, the growth rate began to decrease gradually when austenite grains coarsened obviously. This was because the energy for grain growth can no longer be provided within the remained heating temperature, and the redissolution and ripening of the second phase particles has been basically fixed. Consequently, the pining effect by second phase particles on austenite grain boundaries tended to be stable, so the change of austenite grain size gradually became weak.

3.4. Martensite Transformation

The abovementioned austenite grain growth rules at different quenching temperatures indicate that the austenite grain size greatly varied at different quenching temperatures. It has been pointed out that the austenite grain size affected the martensitic transformation temperature and phase transformation behavior of supercooled austenite during the cooling. Figure 9 records the martensitic transformation during the cooling in the sample with a quenching temperature of 860 °C. Martensite lath appeared, as shown by the blue arrow in Figure 9a, when the temperature decreased to 369.2 °C. This martensite was primary martensite, also called as fresh martensite (FM). The martensitic phase transition point (M_s) of the sample was about 369.2 °C, while the M_s temperature of this steel was determined to be 340 °C by thermal simulation experiment. The difference in the initial temperature of martensitic transformation by two methods was resulted from that the effective M_s was obtained by thermal simulation experiment through the overall volume expansion effect of martensitic

 doi:10.20944/preprints202304.0909.v1

transformation, while in-situ observation determined the M_s just according to the temperature at which the martensite appeared in one certain grain. Generally speaking, the M_s determined by in-situ observation was higher than that reflected in thermal simulation experiments. This is because martensitic transformation did not start at the same time in all grains although the nucleation and growth of martensite explosively proceeded. In addition, martensite nucleated from the grain boundary and grew intragranular until stopped at the grain boundary. More and more martensite laths explosively appeared as the temperature decreased, and most martensite laths traversed the entire grain. Furthermore, some martensitic laths were found to nucleated and grown from the twins (Figure 9b). Since the formed martensite stimulated the nucleation of the surrounding untransformed austenite, the austenite nucleated and grew in parallel after being provoked. Therefore, the martensite laths growing in parallel in some austenite grains. When the temperature decreased to 267.5 ℃, the martensitic laths appeared simultaneously with an angle of 60°. Besides, some martensitic lath synchronously formed paralleling to each other. More FM was found as the temperature continued decreasing accompanied by the secondary martensite (SM). SM referred to the martensite with slightly thin lath formed around FM, which appeared at a certain angle with FM (Figure 9c). More and more surface reliefs due to martensitic transformation gradually appeared at parent austenite grain boundaries and fresh martensite as the increased volume fraction of martensite (Figure 9d). Most martensite stopped growing when they encountered grain boundaries, and some martensite meet each other, which also stop the growth of martensite lath (Figure 9e). The nucleation and growth of martensite were very weak when the temperature closed to room temperature. Most martensite transformation finished within 13 seconds, and the rate of martensitic transformation gradually slowed down. However, the distortion caused by martensitic transformation prevented the martensitic transformation in surrounding austenite. A small part of the regions was retained as residual austenite, in which the allocation of elements such as C in ferrite to residual austenite was mainly completed, due to the failure of martensitic phase transformation (Figure 9f). The growth rate of martensitic lath was relatively fast, but the growth rate of longitudinal martensitic lath was faster than that of lateral ones. Although martensitic transformation explosively proceeded, but the martensitic transformation was not simultaneous. Martensitic transformation selectively started in the parent austenite grain, but this selective process was very short. Nevertheless, the temperature of the sample may remain unchanged or even slightly increase during the cooling process since martensitic transformation released more latent heat of transformation. Therefore, the isothermal martensite formation was inevitable. This latent heat caused by martensitic transformation was also one of the reasons for the selective initiation of martensitic transformation. The supercooling degree became smaller at a constant or slightly increased temperature, thus the martensitic transformation was inhibited. In addition, the selective initiation of martensitic was also related to the distortion caused by the martensitic transformation. The martensitic transformation in untransformed austenite was strongly inhibited by the surrounding martensitic transformation.

Preprints (www.preprints.org) | NOT PEER-REVIEWED | Posted: 25 April 2023 doi:10.20944/preprints202304.0909.v1

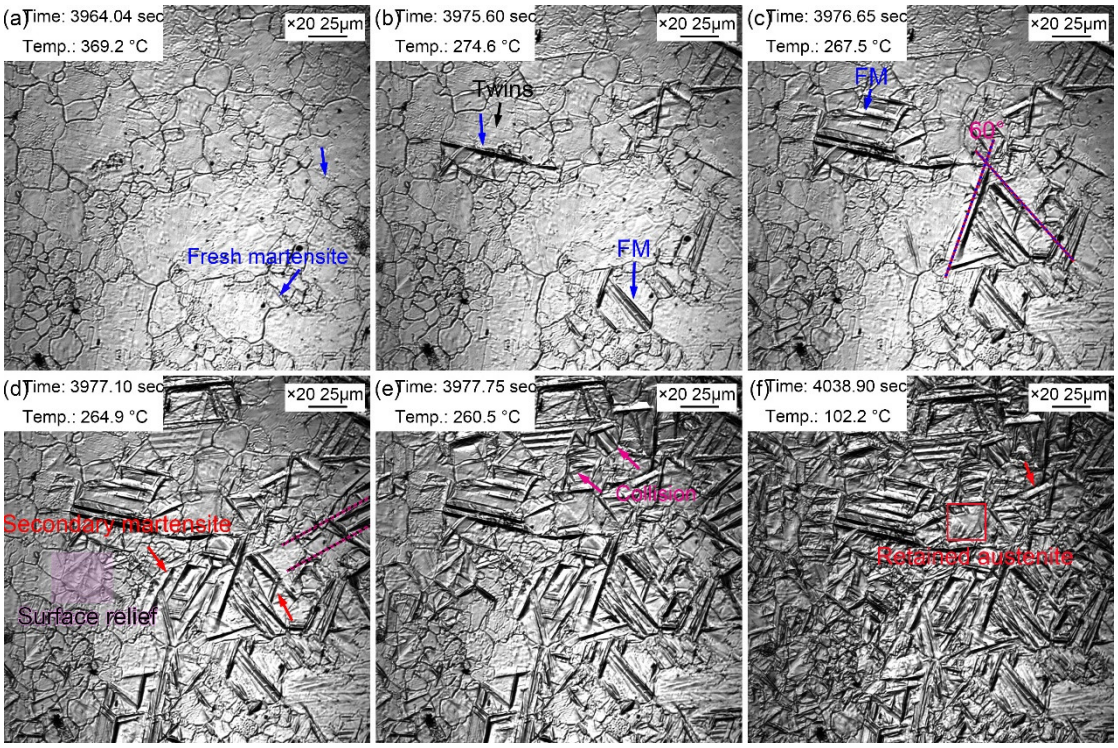

Figure 9. Martensite transformation of supercooled austenite quenched at 860 °C. (**a**) 369.2 °C, martensite appeared; (**b**) 274.6 °C, martensite increased; (**c**) 267.5 °C, martensite nucleated and grew at the twin; (**d**) 264.9 °C, SM and surface relief; (**e**) 260.5 °C, martensitic lath collision; (**f**) 102.2 °C, martensitic transformation stopped, and residual austenite formed.

The martensitic transformation during the cooling process of supercooled austenite with a quenching temperature of 1160 °C is displayed in Figure 10. Martensitic laths appeared at 310.0 °C, as shown by the blue arrow in Figure 10a. It is referred that the martensitic phase transition point M_s was about 310.0 °C, which was lower than that in the sample whose quenching temperature was 860 °C (369.2 °C). Generally speaking, the M_s temperature of martensitic transformation should be higher in a larger austenite. However, the results of in-situ observation of martensitic transformation were extraordinary. The possible reason was that the martensitic transformation observed by in-situ method was on the local of the sample surface, and its view field was limited. The unobserved view field may have undergone the martensitic transformation at a relatively high temperature. In addition, due to the martensitic transformation on the sample surface, it is difficult to unify the different starting temperatures of martensitic transformation due to the uneven composition caused by the evaporation of alloying elements formed during the heating process in austenite. More and more martensitic lath appeared as the temperature decreased. Martensitic lath nucleated from the grain boundary and grew intragranular until stopping at the grain boundary. However, it was accidentally observed that martensitic lath grew through grain boundaries in Figure 10c. The grain boundaries that were passed through were relatively straight, which newly formed during the thermal holding. In addition, some martensitic lath nucleated and grew from the twins. The reason why twins acted as the martensitic nuclei was that martensitic transformation required structural and energy fluctuation. As a kind of crystal defect, twins provided large defect energy to meet the structural and energy fluctuation, to promoted martensitic transformation. Martensitic laths appeared simultaneously at a 60° angle, and some martensitic laths formed synchronously paralleling to each other. More and more FM and SM gradually increased with the decrease of temperature, in which the SM appeared at a certain angle with FM. Most martensite transformation finished within 2.25 seconds, and the rate of martensite transformation slowed down. However, the distortion caused by martensite transformation inhibited the martensite transformation in surrounding austenite (Figure 10j). Martensite growth was a nondiffusion-free interfacial cooperative pushing process, and its specific volume was larger than that of austenite. Therefore, elastic

Preprints (www.preprints.org) | NOT PEER-REVIEWED | Posted: 25 April 2023 doi:10.20944/preprints202304.0909.v1

deformation was caused accompanied by volume expansion during the martensite phase transition. And then large distortion energy formed, which hindering the further martensite transformation.

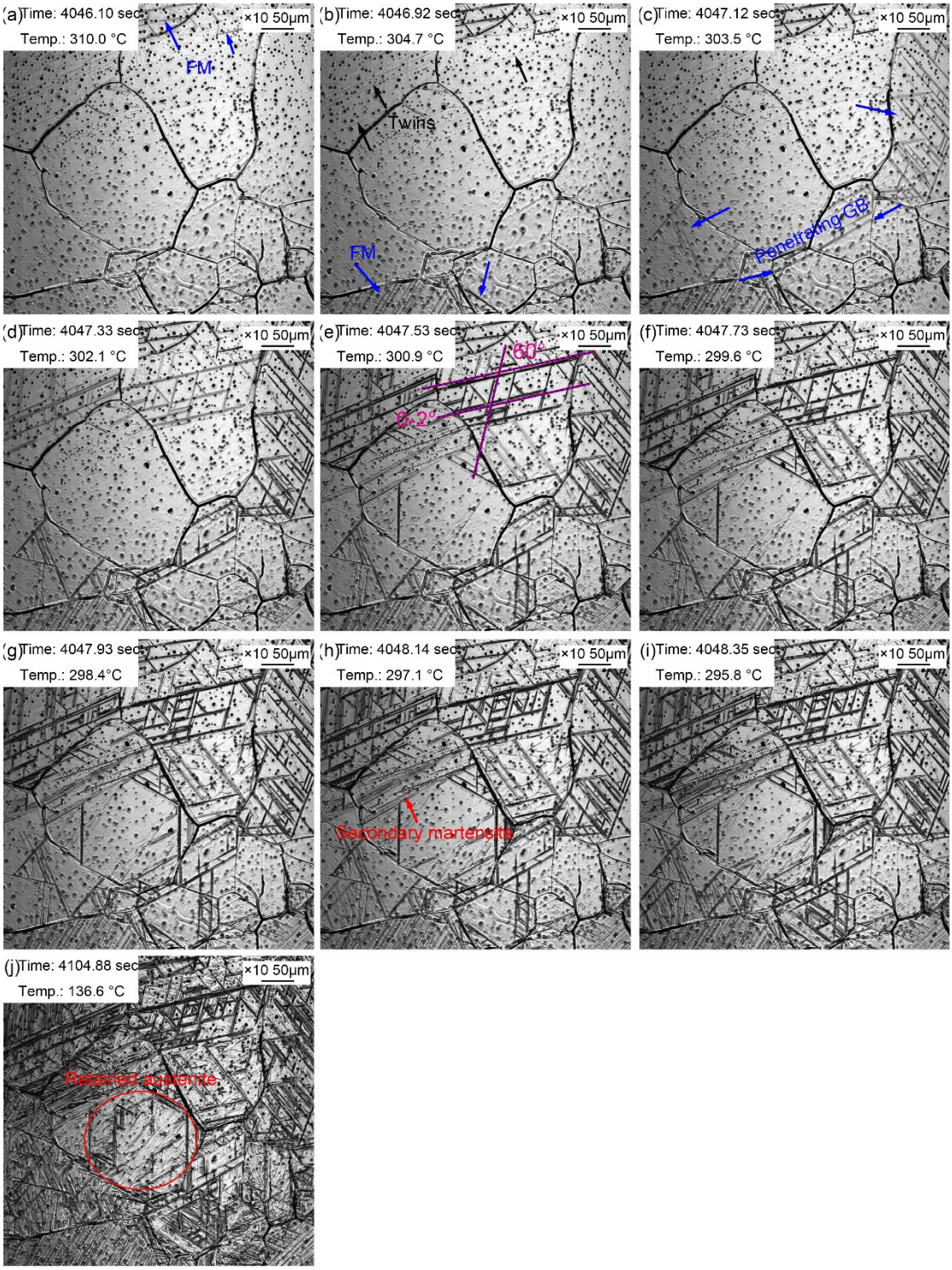

Figure 10. Martensite transformation of supercooled austenite quenched at 1160 ℃. (**a**) 310.0 ℃, martensite appeared; (**b**) 304.7 ℃, martensite increased; (**c**) 303.5 ℃, martensite traversed grain boundary; (**d**) 302.1 ℃, martensite increased and appeared in 60°; (**e**) 300.9 ℃, martensitic packet; (**f**) 299.6 ℃, SM increased; (**g~i**) 298.4 ℃, explosive martensite; (**j**) retained austenite.

According to the in-situ observation of martensitic transformation, martensitic transformation in the same sample did not appear firstly in large size grains, then in small size grains, but appeared in the parent austenite grains in a seemingly chaotic manner. This may be explained by the differences

Preprints (www.preprints.org) | NOT PEER-REVIEWED | Posted: 25 April 2023 doi:10.20944/preprints202304.0909.v1

in the size, composition, and defect density in austenite grains, which leading to the selectivity of martensite nuclei. In addition, the martensitic transformation was also affected by the completed martensitic transformation. For example, the region where the martensitic transformation occurred firstly inhibited the martensitic transformation of the surrounding austenite. And then a certain supercooling degree was required to provide the driving force for the martensitic transformation. Therefore, as the temperature continued decreasing, martensitic transformation began to proceed in other grains. This also explained the phenomenon that the martensitic phase transition increased gradually with the decrease of temperature in the in-situ observation. In addition, it can also be found that FM was larger than SM, and SM usually nucleated and grew attaching to the FM. Compared with the martensitic transformation in the sample at 860 ℃, the martensitic transformation process was faster, and the martensitic lath was longer at a quenching temperature of 1160 ℃. It reflected that the martensitic growth inhibition was less in the large parent austenite grains. Furthermore, the grains were coarser due to higher quenching temperature, thus the driving force of martensitic transformation was greater. And the migration rate of phase interface increased accordingly, so the martensitic transformation was faster.

Figure 11 indicates the martensitic transformation of supercooled austenite at different quenching temperatures, which was summarized based on in-situ observation. Martensite nuclei did not occur synchronously during the quenching process of supercooled austenite, but selectively proceeded and increased in batches in some areas. This nucleation pattern divided untransformed austenite into multiple regions. In different regions, the size of firstly formed martensite (FM) was large, and the size of subsequent martensite (SM) was small. This is because the shape of martensite depended on the stress field between the nucleated martensite laths and other martensitic embryos. The parent phase austenite presented obvious different grain sizes at different quenching temperatures. In addition, the size and volume fraction of the coarsen second phase particles in the matrix increased with the quenching temperature.

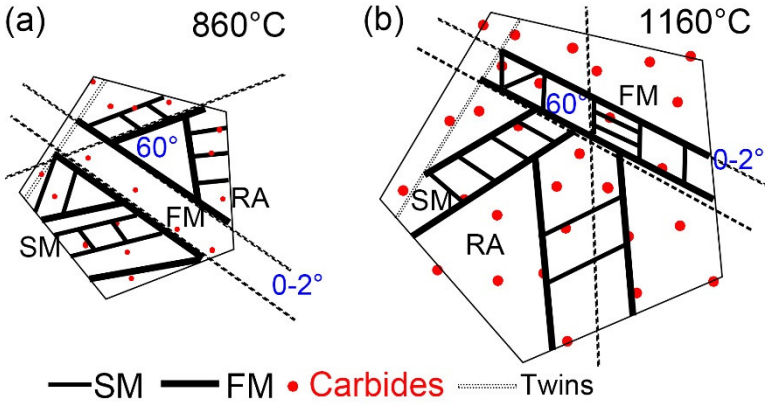

Figure 11. Schematic diagram of martensitic transformation of supercooled austenite at (**a**) 860 ℃ and (**b**) 1160 ℃.

Martensitic nucleation and growth in different parent austenite grains did not affect each other at the early stage of martensitic transformation, during which less martensite formed. The martensitic transformation gradually increased as the temperature decreased, and the martensitic laths restricted each other. In general, there were three types for martensitic nucleation. Firstly, martensite nucleated along the parent austenite grain boundary and grew intragranular until stop growing when it collided other martensitic lath or grain boundary. Besides, martensite nucleated at annealing twins, which had lattice defects and provided better structural and energy fluctuations. Moreover, martensite nucleated at the pre-formed martensite lath and grew into the austenitic grains at about 60° or 120° to form new martensite lath. The lath packet presented two styles: one was the parallel laths (0~2°) based on the pre-formed laths and another was the martensitic laths at 60° or 120° in the other direction stimulated by the pre-formed laths, finally forming the triangle, parallelogram or hexagon morphologies. The size of FM was larger than SM, because FM formed in the parent

austenite without other martensite constraints, while SM only nucleated and grew in the area surrounded by other preformed martensite. The growth space of SM was severely restricted, and the martensite transformation resistance at this stage was greater, resulting in greater elastic stress between martensite laths and the smaller SM laths. The formation of SM laths also strongly inhibited the martensitic transformation of its surrounding untransformed austenite and promoted the formation of residual austenite.

4. Conclusions

(1) The austenite grain at a quenching temperature of 860 ℃ was smaller than those at a quenching temperature of 1160 ℃. Austenite grains coarsened in a short time at a higher quenching temperature of 1160 ℃. In addition, a large amount fine dispersed second phase particles redissolved and ripped at 1160 ℃, resulting in the many large and visible carbonitrides.

(2) The nucleation of martensite did not synchronously proceed during quenching process. The selective prenucleation dominated in martensite nucleation, which dividing untransformed austenite into several regions, and resulting in the larger size of fresh martensite than that secondary martensite.

(3) Martensite can not only nucleate at parent austenite grain boundaries, but also nucleate in the preformed martensite laths and twins. The larger the parent austenite grain size, the smaller constraint in the martensite growth, resulting in the longer fresh martensite and secondary martensite. Besides, the martensite transformation was shorter in a higher quenching temperature. In addition, martensitic lath could traverse the unstable new parent austenitic grain boundaries.

(4) The martensitic laths presented in parallel laths (0~2°) based on the pre-formed lath or distributed in triangle, parallelogram or hexagon with an angle of 60° or 120°.

Funding: The authors gratefully acknowledge the financial support from National Natural Science Foundation of China (No. 52004193), China Postdoctoral Science Foundation (No. 2022M710596) and the Joint Foundation of Nature Science Foundation of Hubei Province (2022CFD078).

Institutional Review Board Statement: Not applicable.

Informed Consent Statement: Not applicable.

Data Availability Statement: The raw/processed data required to reproduce these findings cannot be shared at this time as the data also forms part of an ongoing study.

Conflicts of Interest: The authors declare no conflict of interest.

References

1. Bourithis, L.; Papadimitriou, G.D. The effect of microstructure and wear conditions on the wear resistance of steel metal matrix composites fabricated with PTA alloying technique. *Wear* **2009**, *266*, 1155–1164.
2. Lee K, Nam D H, Lee S, et al. Hardness and wear resistance of steel-based surface composites fabricated with Fe-based metamorphic alloy powders by high-energy electron beam irradiation. *Mater. Sci. Eng. A* **2006**, *428*, 124–134.
3. Wei M X, Wang S Q, Wang L, et al. Effect of microstructures on elevated temperature wear resistance of a hot working die steel. *J. Iron Steel Res. Int.* **2011**, *18*, 47–53.
4. Wang W, Song R B, Peng S G, et al. Multiphase steel with improved impact abrasive wear resistance in comparison with conventional Hadfield steel. *Mater. Des.* **2016**, *105*, 96–105.
5. Du X, Ding H, Kai W, et al. Influence of impact energy on impact corrosion abrasion of high manganese steel. *J. Wuhan Univ. Technol. Mater. Sci.* **2007**, *22*, 412–416.
6. Chen, J.; Wang, J.J.; Zhang, H.; et al Evolution of deformation twins with strain rate in a medium-manganese wear-resistant steel, F.e.–.8.M.n.–.1.C.–.1.2.C.r.–.0.2.V. *J. Iron Steel Res. Int.* **2019**, *26*, 983–990.
7. Si H T, Xiong R L, Song F, et al. Wear resistance of austenitic steel Fe-17Mn-6Si-0.3C with high Silicon and high Manganese. *Acta Metall. Sin.* **2014**, *27*, 352–358.
8. Yong Liu, Yongfang Tang, Ganghan Huang. Improvement of mechanical properties of low alloy steel with high strength and wear resistance. *J. Iron Steel Res.* **1999**, *3*, 79–81. (In Chinese)
9. Zumelzu E, Goyos I, Cabezas C, et al. Wear and corrosion behaviour of high Cr cast iron alloys. *J. Mater. Process. Technol.* **2002**, *128*, 250–255.

10. Zhang A, Xing J, Fang L, et al. Inter-phase corrosion of chromium white cast irons in dynamic state. *Wear* **2004**, *257*, 198–204.
11. Tian H H, Addie G R, Visintainer R. Erosion–corrosion performance of high-Cr cast iron alloys in flowing liquid–solid slurries. *Wear* **2009**, *267*, 2039–2047.
12. Huifeng Chen, Jingxia Hu. Study on Carbides of High Chromium Cast Iron. *J. Shanghai Inst. Technol. Nat. Sci. Ed.* **2003**, *3*, 57–62. (In Chinese)
13. Xiaoming Cui, Ning Wang, Pei Gong, Hao Yang, Pucun Bai. Effect of C, Cr contents and heat treatment on the microstructure and mechanical properties of high chromium cast iron. *J. Inn. Mong. Univ. Technol.* **2016**, *4*, 277–282. (In Chinese)
14. Tkowska, B.; Dziurka, R.; Baa, P. Analysis of phase transformations of supercooled austenite in low-alloy steel with boron additives. *Met. Sci. Heat Treat.* **2016**, *57*, 525–530.
15. Liu Q D, Wen H M, Zhang h, et al. Effect of multistage heat treatment on microstructure and mechanical properties of high-strength low-alloy steel. *Metall. Mater. Trans. A* **2016**, *47*, 1960–1974.
16. Xu X, Ederveen F H, Sybrand V, et al. Correlating the abrasion resistance of low alloy steels to the standard mechanical properties: A statistical analysis over a larger data set. *Wear* **2016**, *368*, 92–100.
17. Sundström, A.A.; José, R.; Olsson, M. Wear behaviour of some low alloyed steels under combined impact-abrasion contact conditions. *Wear* **2001**, *250*, 744–754.
18. Fu, H.; Xiao, Q.; Fu, H. Heat treatment of multi-element low alloy wear-resistant steel. *Mater. Sci. Eng. A* **2005**, *396*, 206–212.
19. Kaijalainen A J, Suikkanen P P, Limnell T J, et al. Effect of austenite grain structure on the strength and toughness of direct-quenched martensite. *J. Alloys Compd.* **2013**, *577*, 642–648.
20. Zhang C Y, Wang Q F, Kong J L, et al. Effect of martensite morphology on impact toughness of ultra-high strength 25CrMo48V steel seamless tube quenched at different temperatures. *J. Iron Steel Res. Int.* **2013**, *20*, 62–67.
21. Liang Y L, Long S L, Xu P W, et al. The important role of martensite laths to fracture toughness for the ductile fracture controlled by the strain in EA4T axle steel. *Mater. Sci. Eng. A* **2017**, *695*, 154–164.
22. Fazaeli, A.; Ekrami, A.; Kokabi, A.H. Microstructure and mechanical properties of dual phase steels, with different martensite morphology, produced during TLP bonding of a low C-Mn steel. *Met. Mater. Int.* **2016**, *22*, 856–862.
23. Li, S.; Zhu, G.; Kang, Y. Effect of substructure on mechanical properties and fracture behavior of lath martensite in 0.1C-1.1Si-1.7Mn steel. *J. Alloys Compd.* **2016**, *675*, 104–115.
24. Yilong Liang, Min Lei, Shuhui Zhong, Shan Jiang. The relationship between fracture toughness and notch toughness, tensile ductilities in lath martensite steel. *Acta Metall. Sin.* **1998**, *9*, 950–958.
25. Inoue T, Matsuda S, Okamura Y, et al. The fracture of a low carbon tempered martensite. *Trans. JIM* **1970**, *11*, 36–43.
26. Zhenjia Xie, Chengjia Shang, Wenhao Zhou, Binbin Wu. Effect of retained austenite on ductility and toughness of a low alloyed multi-phase steel. *Acta Metall. Sin.* **2016**, *2*, 224–232.
27. Gaofei, Liang, Zhenming Xu, Jianguo Li, Qichuan Jiang. The latest development of anti-wear steel. *Spec. Steel* **2002**, *23*, 1–7.
28. Yi Cao, Zhaodong Wang, Zaiwei Jiang, Ti Zhang, Chao Wang, Di Wu. Development and research of wear-resistant steel with high strength and toughness. *Steel Roll.* **2011**, *28*, 3–7.
29. Ma Y P, Li X L, Wang C H, et al. Microstructure and impact wear resistance of TiN reinforced high manganese steel matrix. *J. Iron Steel Res. Int.* **2012**, *19*, 60–65.
30. NLiu, Z.D. Liu, X.K. He, Z.Q. Yang, Austenite transformation of SA508Gr.4N steel for nuclear reactor pressure vessels during heating process. *Heat Treat. Met.* **2017**, *42*, 88–92.
31. Qing Yuan, Jie Ren, Jiaxuan Mo, Zhicheng Zhang, En Tang, Guang Xu, Zhengliang Xue. Effects of rapid heating on the phase transformation and grain refinement of a low-carbon mciroalloyed steel. *J. Mater. Res. Technol.* **2023**, *23*, 3756–3771.
32. Agren, G.P. Vassilev, Computer simulations of cementite dissolution in austenite. *Mater. Sci. Eng.* **1984**, *64*, 95–103.